NANO LETTERS

Letter

pubs.acs.org/NanoLett

Entropy-Mediated Mechanical Response of the Interfacial Nanoparticle Patterning

Zhengyang Liu,† Ruohai Guo,† Guoxi Xu, Zihan Huang, and Li-Tang Yan*

Key Laboratory of Advanced Materials (MOE), Department of Chemical Engineering, Tsinghua University, Beijing 100084, People's Republic of China

Supporting Information

ABSTRACT: The precise organization of nano-objects into well-defined patterns at interfaces is an outstanding challenge in the field of nanocomposites toward technologically important materials and devices. Herein, by means of computer simulations we show novel mechanomutable nanocomposites designed by binary mixtures of tethered Janus nanoparticles at the interface of a binary fluid mixture under mechanical pressure. Our simulations demonstrate that the nanoparticle organization in the systems undergo reversible transition between random state and long-ranged intercalation state, controlled by various structural parameters of the tethered chains and the applied pressure. The dynamical mechanism during the transition is explored through examining the diffusion trajectories of the nanoparticles confined at the interfaces. We provide a theoretical analysis of the lateral pressure induced by the tethered chains, which is fully supported by simulation data and reveals that the compression-induced transition is fundamentally attributed to the entropic effect from the tethered chains. Our study leads to a class of interface-reactive nanomaterials in which the transfer and recovery of interfacial nanopatterning presents precise and tunable mechanical responses.

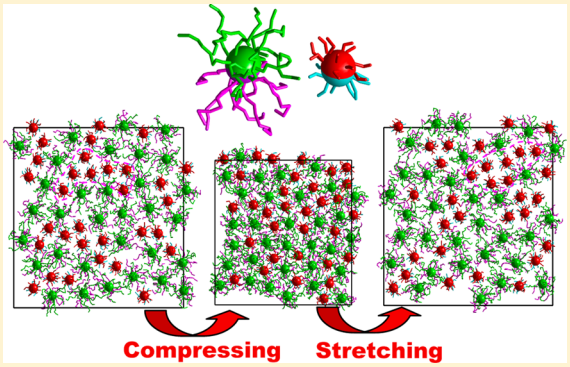

KEYWORDS: *Interfacial nanopatterning, mechanical response, tethered Janus nanoparticle, entropy-mediated effect, intercalated nanostructure, computer simulation*

Predicting the behavior of nanoparticles at surfaces and interfaces is an important ability relating to the design of novel nanostructured materials, where polymer nanocomposites play an increasingly important role,[1−6] but also to a better understanding of many biological systems,[7−9] where nanoscale objects such as viruses or proteins can interact with various interfaces. Of particular interest is to develop novel and efficient design routines to direct the interfacial organization of multicomponent nanoparticles toward a high degree of order and even responsive behaviors to certain external stimuli.[10−15] Examples are flexible sensors,[15] tunable plasmonic nanostructures,[16] ultrafast switches and organic memory devices,[17] and advanced photovoltaic devices.[18] However, the issues that determine the mechanisms of collective organization for the nanoparticles confined at a fluid−fluid interface and, particularly, how their structural or phase transition responds to applied stimuli, remain largely unresolved even from an empirical perspective. Importantly, it is a great challenge to dynamically tune the interfacial nanopatterns formed by the self-assembly of multicomponent nanoparticles because the cooperative organization and stimuli-response behaviors of these nanoparticles at fluid interfaces are governed by complicated thermodynamic nature as well as kinetics.[12,19−22]

This work thereby addresses a major challenge in the field: how to dynamically organize the multicomponent nanoparticles confined at the fluid interfaces. Generally, structurally complex organization of nanoparticles can be obtained employing macromolecules as templates including DNA,[23] linear polymers,[24] and block copolymers.[25,26] While remarkable and oftentimes useful in the bulk or at surfaces, these strategies are limited at the fluid−fluid interfaces. A potential principle to address the challenge may turn to exploring and taking advantage of specific entropic origins, as controllable entropic contribution keeps springing nonintuitive findings in the manipulation of hierarchical structures formed in many soft matter systems containing nanoparticles.[27−30] Little however has been explored about the application of entropic factors in the organization of multicomponent nanoparticles confined at the fluid interfaces. Albeit challenging, effective control using the interplay between thermodynamic interactions and external stimuli to direct the ordering and responsive behaviors of multicomponent nanoparticles at fluid interfaces is undoubtedly important due to the great flexibility offered by such systems to manufacture new materials.

Herein, we demonstrate an entropy-mediated, responsive, and tunable nanoparticle organization arising from collective

Received: July 31, 2014
Revised: October 27, 2014
Published: November 6, 2014

   dx.doi.org/10.1021/nl5029396 | *Nano Lett.* 2014, 14, 6910−6916

behavior of binary nanoparticle mixtures at the fluid−fluid interface, where the two components of nanoparticles are chosen as Janus nanoparticles with amphiphilic surface chemically modified by the tethered ligand chains. Through applying mechanical pressure, the systems exhibit mechanical response characterized by the reversible transition between random state and long-ranged intercalation state of different nanoparticle components. We study what are the fundamental conditions necessary to induce and control the compression-induced transition of the nanoparticle patterns at the fluid interfaces by systematic computer simulations and theoretical analysis. This allows us to reveal the detailed dynamics and the entropic effect resulting in the novel phenomena in origin.

Full technical details on the simulation method and the models of tethered Janus nanoparticles are described in Method Section. Briefly, computer simulations are carried out using dissipative particle dynamics (DPD), a method that samples the *NVT* ensemble.[31] Each Janus nanoparticle consists of two symmetry surface sites functionalized by the tethered ligand chains.[32−35] Two components of Janus nanoparticles involved in the system are identified by the difference in the length of tethered chains [Figure 1a], which induce repulsive interaction between the different nanoparticle components. We consider an *AB* binary fluid mixture where two components undergo a relatively strong phase separation that leads the system to segregate into two domains with a flat interface whereas the results demonstrated here may apply to wider mixtures with more complicated interfacial topologies. Chain lengths are expressed in total number of DPD beads connected together in the chain. Here, L_A (L_P, L_Q) = 8 and L_B (L_p, L_q) = 2 are set for the long and short tethers, respectively. The tethering density of Janus nanoparticle, w, is set to about 0.028 chains/r_c^2, where r_c is the truncate distance of the forces. The radius of a bare nanoparticle is fixed at 1.12r_c. As an example, the total number of 64 tethered Janus nanoparticles with equal number for two components are randomly positioned at the fluid interface for the initial simulations [Figure 1b]. Specially, mechanical pressure is exerted to the system by changing the lateral dimensions of our simulation box and simultaneously modifying the height of the box to keep the volume of the system constant, that is, $(x, y, z) \rightarrow (\delta x, \delta y, z/\delta^2)$, as indicated by the arrows in Figure 1b.[36]

To quantify the interfacial nanoparticle organization, we use the mixing parameter, φ, defined by $\varphi = N_{ls} - N_{ll} - N_{ss}$, where N_{ls}, N_{ll}, and N_{ss} are number fractions of line contacts between unlike nanoparticle pairs and like pairs for the nearest neighboring nanoparticles determined by the Delaunay triangulation.[37] The highest φ value approaches about 0.33, expected for the perfect intercalation state of the present nanoparticle mixtures. Generally, there are three basic mixing states as demonstrated by the images in Figure S1, that is, phase-separated state, randomly mixing state, and the intercalated state with perfect mixing. In the absolutely phase-separated state ($\varphi = -0.95$), two components segregate from each other, leading to the formation of big phase domains and obvious phase interface between two different phase domains. In the randomly mixing state ($\varphi \approx 0.03$), although the two components take a better mixing than the phase-separated state, there are still phase domains of the same nanoparticle component, as marked by the dashed pink circles in Supporting Information Figure S1e. The most perfect mixing state of the nanoparticle mixtures occurs in the intercalated state (φ = 0.33), where two nanoparticle components present a perfectly

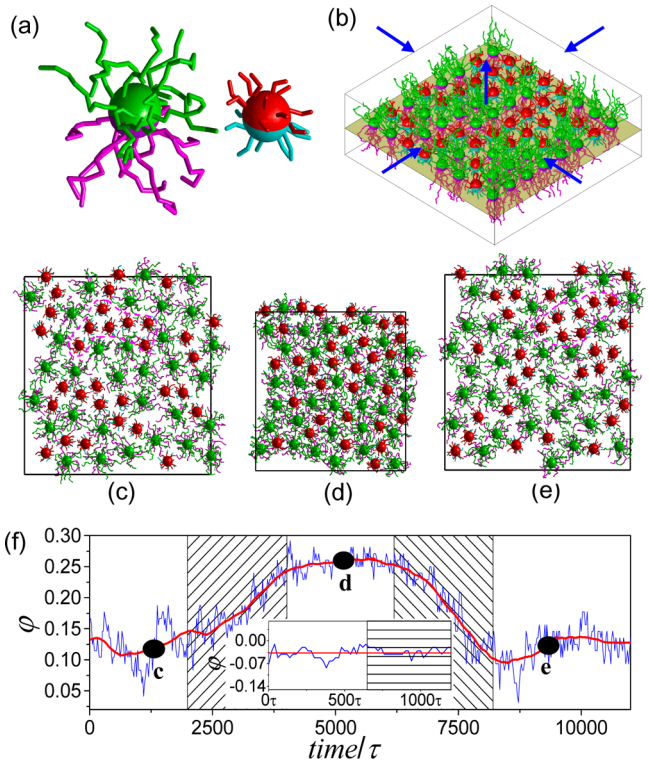

Figure 1. (a) Janus nanoparticles tethered with long and short ligand chains. (b) The random arrangement of nanoparticles at the fluid interface for the initial simulations. The dark yellow surface represents the fluid interface whereas the fluid beads are not shown for clarity. The arrows indicate the lateral and vertical changes of the simulation box during applying a mechanical pressure. (c−e) Top-view snapshots of the interfacial nanoparticle patterns at the times denoted by the black points in (f), where $S = S_0$ (c), $S = 0.64S_0$ (d), and $S = S_0$ (e). The dashed circles in (c,e) highlight the phase domains of the same nanoparticle component. (f) The time dependence of φ during a successive compressing-stretching process for the system with L_A = 8 and L_B = 2. The left and right rectangles mark the compressing and stretching processes, respectively. The inset shows φ during a compressing process, as marked by the rectangle, for the system with $L_A = L_B$ = 8. Details of the process with more snapshots can be found in Supporting Information Figures S2 and S5.

intercalated mixing. A higher φ value indicates a better mixing for the two nanoparticle components (for more details of φ, see Supporting Information 1 and Figure S1). The system with a lower φ value instead tends to phase separation.

After equilibration of the initial system demonstrated in Figure 1b, the fluid−fluid interface is found to keep flat with the equator of Janus nanoparticles coinciding with the interface and the tethers being in their favorable phase domains. However, we find that obvious deformation of the interface can be induced when the system is compressed beyond a critical point (that is, the interfacial compression ratio $\lambda > 0.2$), which is avoided in the present simulations so that we can determine the detailed relation between the spatial organization of interfacial nanoparticles and the lateral compressing pressure. Actually, complex defect motifs of the spatial organization of nanoparticles will be generated on the deformed interfaces.[38,39] An approximately randomly mixing state, as evidenced by φ = 0.12, is isolated from the top-view snapshot of the equilibrium system [Figure 1c and Supporting Information Video 1], where the nanoparticle components form irregular phase domains as marked by the dashed circles. A little higher value of φ than

dx.doi.org/10.1021/nl5029396 | *Nano Lett.* 2014, 14, 6910−6916

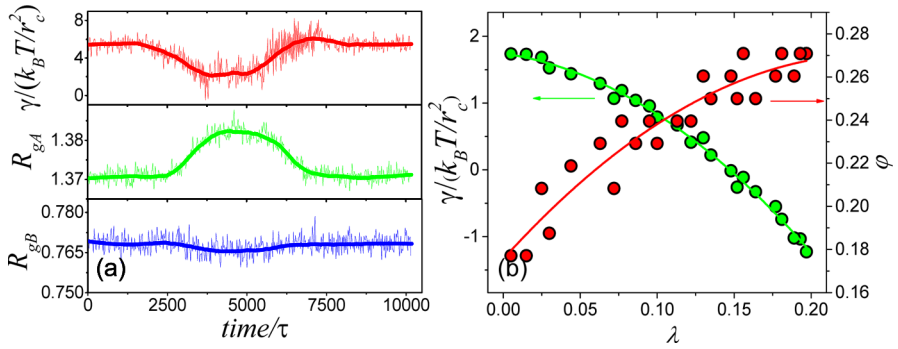

Figure 2. (a) The time dependence of the surface tension, γ, and radii of gyration of the long and short tethers, R_{gA} and R_{gB}, during the compressing-stretching process corresponding to Figure 1. k_B is the Boltzmann constant. (b) The relations of γ and φ to the interfacial compression ratio, λ. The solid lines are used to guide the eye.

that of the purely random mixing state ($\varphi \approx 0.03$) is due to the lightly compressing state chosen at the initial time.

We then examine the mechanical responsive behaviors of the interfacial nanoparticle organization by exerting a programmed mechanical pressure to the system. First, the equilibrium system is compressed so that the interface area S is gradually reduced from its initial value, S_0, to $0.64S_0$. After an equilibration stage, the compressed system turns to be mildly stretched until S returns to S_0. The fluid interface is confirmed to remain flat during the whole process. The red plot in Figure 1f shows how φ responds as the system with a sufficient disparity in tether lengths, that is, $L_A = 8$ and $L_B = 2$, undergoes such a compressing-stretching process. The plot section within the left rectangle demonstrates that a significant increase of φ is induced during the compressing process (for details of the compressing process, see Supporting Information Video 2). The value of φ remains stable at almost 0.28 after ceasing the compression, indicating a good intercalation state formed by the different nanoparticle components. The increase in φ, corresponding to the enhanced contacts between unlike nanoparticle pairs, is consistent with the visual observation of the nanoparticle pattern shown in Figure 1d where the big nanoparticle domains disappear and the two components indeed present a long-ranged intercalation state.

In the stretching process as marked by the right rectangle, we see that φ turns to decrease as the interfacial area is enlarged (for details of the stretching process, see Supporting Information Video 3). After ending the stretching process, it is interesting to find that φ returns to its original value before the compressing process. A representative snapshot at this stage, that is, Figure 1e, displays a very similar nanoparticle organization with Figure 1c, confirming that the binary nanoparticle components return to the randomly mixing state. This state cycle can be repeated although the result is not shown here for simplicity. All these results demonstrate that the organization of binary tethered Janus nanoparticles at the fluid interface behaves reversible mechanical response to applied pressure, exhibiting a compression-induced transition between random state and long-ranged intercalation state. The reversible transition described in the paper focuses on the two states, that is, randomly mixing state and intercalated state. We do not refer to the phase-separate state because a stable phase-separating state is very difficult to realize in the simulations. Generally, this state will quickly evolve into a randomly mixing state where the φ tends to be 0 because the hydrophilic interaction of the tethers with solvent significantly influences the interaction between tethers (Supporting Information Figure S3). The Brownian motions of the tethered nanoparticles at the enlarged interface can also disturb the formation of a big phase domain (Supporting Information Figure S4).

To explore the effect of the disparity in tether lengths, we compress the binary Janus nanoparticle components with equal tether lengths, that is, $L_A = L_B = 8$. The plot describing the time dependence of φ is shown in the inset of Figure 1f and Supporting Information Figure S5. By comparing with the φ value at $L_A = 8$ and $L_B = 2$, we note that φ becomes much lower due to the occurrence of obvious phase separation between the two nanoparticle components. What is interesting is that the value of φ keeps almost unchangeable and the interaction state does not occur throughout the compressing process (see also the snapshots in Supporting Information Figure S5). Clearly, the compression-induced state transition disappears for the Janus nanoparticles with equal tether lengths. To confirm this conclusion, we also consider the system of $L_A = L_B = 2$ undergoing a similar compressing-stretching process to the system of $L_A = 8$ and $L_B = 2$. Also, no state transition can be identified during the whole process (see Figure S6 and Supporting Information Videos 4–6). These results underscore the important role of sufficient tether disparity in the mechanical response of the system and will be discussed in more detail in the section of mechanism analysis.

We further consider the mechanical response behavior through examining different parameters during the compressing-stretching process. The top plot in Figure 2a shows the result of surface tension, γ, indicating that the applied mechanical pressure induces an obvious response of the surface tension of the system. In Figure 2b, we summarize γ and φ as a function of the interfacial compression ratio, λ, defined by $\lambda = [(S_0)^{1/2} - (S)^{1/2}]/(S_0)^{1/2}$. Increasing λ from 0 to 0.2 results in the increase of φ from 0.12 to almost 0.28 but the decrease of γ from 1.9 k_BT/r_c^2 to −1.2 k_BT/r_c^2, demonstrating the robust responsive ability of the interfacial nanoparticle mixture to the mechanical pressure. Further compressing the system will however induce notable fluctuation of the fluid–fluid interface. By calculating the radius of gyration, R_g, we also present in Figure 2a the changes of tether sizes during the compressing–stretching process. Compressing the system leads to a significant increase of the size of the long tethers and a reverse change exhibits in the stretching process. By comparison, one can find that the long tethers exhibit a larger change than the short ones, which remain nearly constant. Because R_g is an indirect measure of conformational entropy available to the tethers,[29] this reveals that the long tethers provide a larger entropy contribution to the mechanical response.

dx.doi.org/10.1021/nl5029396 | Nano Lett. 2014, 14, 6910–6916

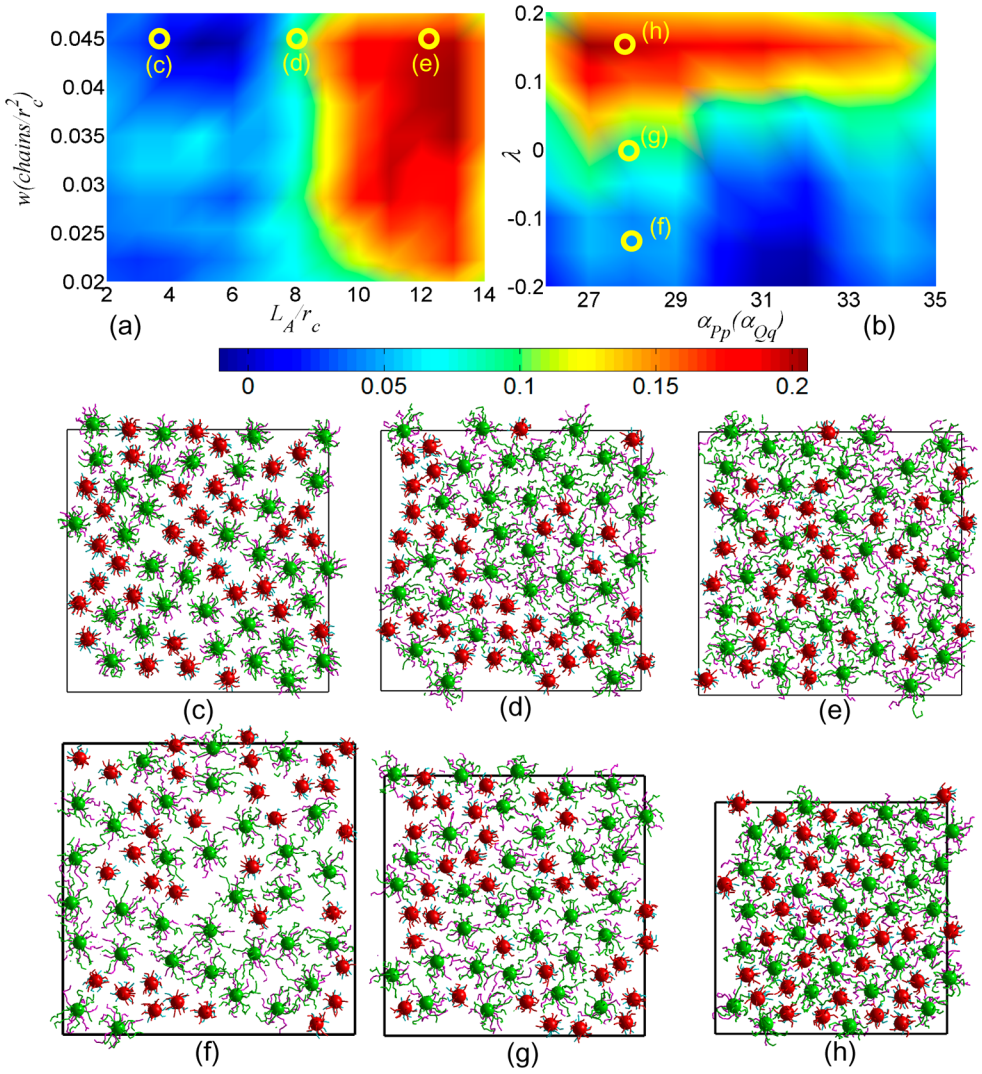

Figure 3. (a) The mixing parameter φ as a function of the tethering density, w, and the length of the long tethers L_A, where the compression ratio $\lambda = 0$, the interaction parameter between the long and the short tethers α_{Pp} (α_{Qq}) = 27, and $L_B = 2$. (b) φ as a function of λ and α_{Pp} (α_{Qq}), where $w = 0.028$ chains/r_c^2, $L_A = 8$, and $L_B = 2$. Note that a negative value of λ indicates a stretched system. The color bar indicates the values of φ. The snapshots of (c–h) exhibit the representative interfacial patterns at various conditions as marked by the points in (a,b).

To explore effective approaches to control the mechanical response behavior, we systematically compute the mixing parameter φ as a function of the tethering density w and the length of the long tethers L_A, and of the compression ratio λ, and the interaction parameter between the long tethers, α_{Pp} (α_{Qq}), which allow us to construct the φ landscapes, plotted by the colored contour map, in the w-L_A and λ–α_{Pp} planes [Figure 3a,b]. Figure 3a and the representative snapshots of Figure 3c–e clarify a strong dependence of the interfacial nanoparticle organization on the length of the long tethers. Only when L_A is no lower than a critical value (about 8 for the current system) can the obvious intercalation state occur. The nanoparticles with shorter tethers yet prefer the random state because they possess sufficient free space to avoid the interparticle repulsion (see also Supporting Information Videos 4–6). The critical value relating to the characteristics of the tethered Janus nanoparticles as well as to the fluid phase properties will be discussed in a forthcoming publication. Figure 3a also shows that altering the tethering density w has a trivial effect on the random state of the interfacial nanoparticles when the length of the long tethers is below the critical value. Once w gets across the critical value, the effect of the tethering density spontaneously becomes stronger. The dark red region on the right top demonstrates that the binary Janus nanoparticles with a high tethering density are prone to the intercalation state because the energetic contribution from the densely tethered chains is significantly enhanced.

Figure 3b and the representative snapshots of Figure 3f–h confirm in a wider scale our previous observation that increasing the compression ratio leads to a better intercalation state of the binary nanoparticle components [e.g., Figure 2b]. Interestingly, we find that this φ–λ relation is particularly remarkable for the weak repulsion between long tethers, that is, a low α_{Pp} (α_{Qq}). At a large α_{Pp} (α_{Qq}), the strong repulsion between long tethers tends to drive the segregation between two nanoparticle components and thereby inhibits the increase of the φ value. As revealed in the later section that the intercalation state is dominated by the entropic contribution, altering α_{Pp} essentially modifies the contest between the enthalpic and the entropic interactions. The enthalpy wins only for an extremely large α_{Pp}, as demonstrated in Figure 3b.

dx.doi.org/10.1021/nl5029396 | Nano Lett. 2014, 14, 6910–6916

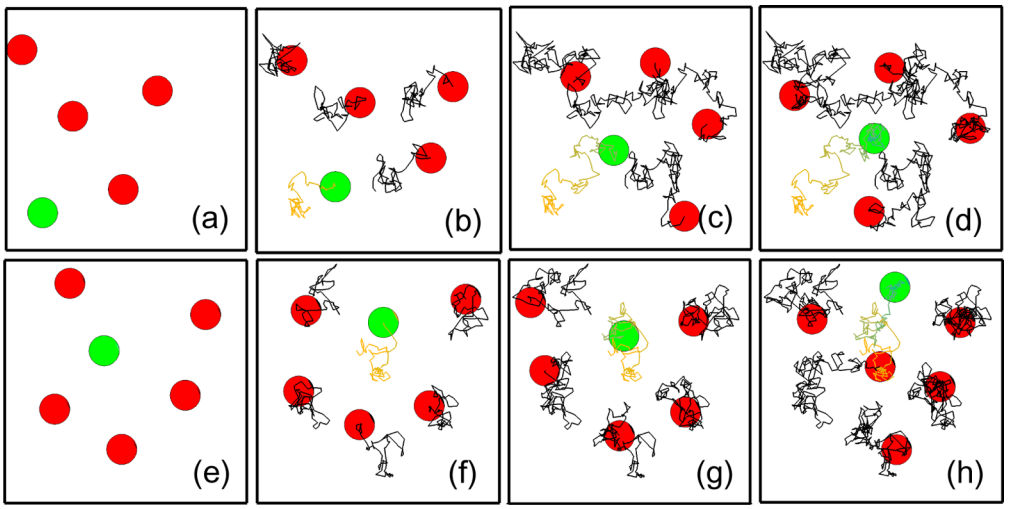

Figure 4. Representative trajectories for the two nanoparticle components during the compressing (a–d) and stretching (e–h) processes. In the compressing process, the system is compressed from $\lambda = 0$ to 0.2 while from $\lambda = 0.2$ to 0 in the stretching process. The red and green circles represent the Janus nanoparticles tethered with short and long chains that are not shown for clarity. The time interval between two neighboring snapshots is 240τ. The curves monitor the detailed trajectories for the center-of-mass of corresponding nanoparticles.

Next we turn to the detailed dynamics during the compressing-stretching process. Actually, the dynamics of nanoscale objects confined in a two-dimensional (2D) plane are very complex and are not well understood.[40−42] The current system offers an ideal model to probe this issue. Figure 4 presents time series of local snapshots showing the 2D diffusion of some neighboring nanoparticles at the fluid interfaces during the compressing and stretching processes. Also, Supporting Information Videos 2 and 3 present more detailed dynamical processes during the compressing and stretching stages, respectively. At the initial time of the compressing process, a short-tether nanoparticle denoted by the green circle is out of the domain formed by four long-tether nanoparticles denoted by the red circles [Figure 4a]. Upon the mechanical compression, the cooperative motion of nanoparticles takes place: the short-tether nanoparticle travels to the nanoparticle domain and spontaneously the long-tether nanoparticles adjust their positions to generate space for its entry into the domain center. This leads to the formation of a typical intercalated unit where the short-tether nanoparticle is caged by the long-tether nanoparticles [Figure 4d]. Figure 4e–h shows the detailed "escaping" process of a short-tether nanoparticle from the cage of the long-tether nanoparticles when the system is stretched. In particular, we do not find evident heterogeneous fluctuations,[40,42] for example, the activated hopping, after examining the detailed diffusion trajectories of the nanoparticles throughout the compressing and stretching processes, although the heterogeneous fluctuations are popular in the diffusion dynamics of some other nanoparticle systems with 2D confinement.[40,42] This may be ascribed to the high adsorption energy from the amphphilic tethers that damp the extreme motion of nanoparticles in the lateral direction.[43] Thus, the interfacial Janus nanoparticles are diffusive predominantly by means of the cooperative motion of particles, as demonstrated in Figure 4.

Finally, we determine the mechanism driving the collective organization of the binary Janus nanoparticles at the fluid–fluid interface by theoretically analyzing the relation between the lateral pressure and the conformational behaviors of the tethers. For this purpose, we consider the lateral pressure, Π, of systems containing a single type of nanoparticles. Π is defined as the reduction of interfacial tension below that of pure binary fluid. In Figure 5a, we show the lateral pressure as a function of the

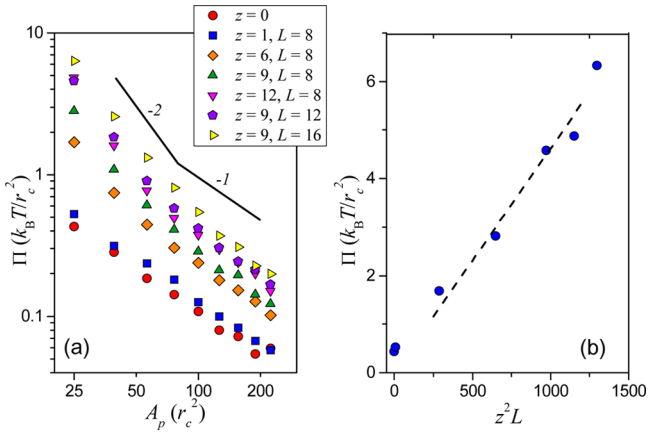

Figure 5. (a) Log–log plots of lateral pressure, Π, versus area per particle, A_p, for various systems denoted by the legend. The solid lines with slopes of −2 and −1 are to guide the eye. (b) Π as a function of z^2L at $A_p = 25r_c^2$. Data points are extracted from systems the same as in (a). Also indicated is the fitting line of the data.

area per particle at the interface, A_p, for various systems in which nanoparticles are tethered with z chains of length L on each surface site. For densely tethered nanoparticles ($z \geq 6$), A_p is sufficiently high before compression, thus the nanoparticles behave like ideal gas molecules.[44] In this case, the lateral pressure changes with A_p as

$$\Pi \propto A_p^{-1} \tag{1}$$

Upon applying mechanical pressure, the tethered chains repel each other, forcing them to extend perpendicular to the interface. For small A_p and long tether length, the tethered chains can be assumed as adopting conformation of a planar brush.[45] When the system is compressed, the concentration of the tethered chains is significantly increased. In this case, the tethered chains behave very like ideal chains because the

dx.doi.org/10.1021/nl5029396 | Nano Lett. 2014, 14, 6910–6916

interactions between monomers are almost completely screened by surrounding chains in the concentrated polymer solutions.[46] Thereby, our theoretical analysis is based on the model of ideal chain, where the internal energy of polymer chains does not change under the lateral compression since the ideal chains behave as linked monomers without interaction energy due to the screening effect as stated above.[45] The corresponding free energy per area of particle, F, can be given by

$$F \approx k_B T \frac{2z^2 L b^2}{A_p} \tag{2}$$

Other contributions to the free energy are much smaller and can thereby be omitted. Hence, the lateral pressure is calculated as

$$\Pi = -\frac{\partial F}{\partial A_p} \approx k_B T \frac{2z^2 L b^2}{A_p^2} \tag{3}$$

As shown in Figure 5a, the lateral pressure indeed scales as A_p^{-2} for small values of A_p. For bare nanoparticle ($z = 0$) and sparsely tethered nanoparticle ($z = 1$), the interaction of nanoparticles is so weak that the lateral pressure can be described by the power law of eq 1 within the whole scale of A_p considered. Figure 5b shows the lateral pressures of systems at $A_p = 25r_c^2$. It is interesting to note that the lateral pressure increases with z^2L linearly, as predicted by eq 3. These results indicate that the ideal chain model is reasonable and the scaling analysis demonstrates the entropy effect from the deformed tethered chains plays a significant role in the collective organization of the interfacial nanoparticles. Under the lateral compression, the long tethers behave like a planar brush in their favorable domains, resulting in a great decrease of conformation entropy. Therefore, the spontaneously transition to long-ranged intercalation state occurs in the binary nanoparticles with sufficient tether disparity to reduce the steric repulsion between long tethers and, fundamental, to increase their conformational entropy since the intercalated short-tether nanoparticles provide additional space facilitating the deformation of the long tethers. Given that binary nanoparticles with equal tethers cannot generate such entropy effect, the analysis thus highlights the important role of the sufficient tether disparity in the mechanical response of the system, as proved by the inset of Figure 1f.

In summary, we demonstrate novel entropy-mediated mechanical response behavior emerging from binary mixtures of tethered Janus nanoparticles at the interface of a binary fluid mixture under mechanical pressure, whereas the results demonstrated here can apply to wider mixtures with more complicated interfacial topologies. The nanoparticle organization in the systems exhibits reversible transition between random state and long-ranged intercalation state that can be effectively controlled by various structural parameters of the tethered chains and the applied pressure. The dynamics mechanism of the transition is explored by examining the detailed trajectories of the interfacial nanoparticles during their 2D diffusion. We have also explained the origin driving the collective organization of the binary Janus nanoparticles at the fluid−fluid interface by combining computer simulations and theoretical analysis and have revealed that both conformational entropy effect of the tethered chains and sufficient tether disparity dominate the collective nanoparticle organization in the mechanical response behavior. The attractive feature of the procedure that we propose is that the interfacial nanostructures are tuned simply by pressing an accessible system containing binary tethered Janus particles in a binary fluid. The motif and findings described in this letter thereby suggest a facile route to create well-defined, responsive, and flexible nanopatterns formed by multicomponent nanoparticles in the interface of wide fluid mixtures and consequently lead to a class of interface-reactive nanocomposites toward technologically important materials and devices. Recalling that the surface structures drastically influence the interactions of nanoparticles with biomembranes,[29,47] it would be interesting to explore to what extent the entropy-mediated mechanical response behavior plays a role in biological systems.

APPENDIX: DPD METHODS AND SIMULATION DETAILS

Computer simulations are carried out using dissipative particle dynamics (DPD), a method that samples the *NVT* ensemble.[31] DPD is a coarse-grained molecular dynamics (CGMD) method and has been successfully used in the simulation of various soft matter systems containing nanoparticles.[32,48] In DPD, the temporal evolution of each particle is governed by Newton's equation of motion, generating the true dynamics. A bead i at position $\mathbf{r}_i$ surrounded by beads $j \neq i$ at $\mathbf{r}_j$ (distance vector $\mathbf{r}_{ij} = \mathbf{r}_i - \mathbf{r}_j$ and unit vector $\mathbf{e}_{ij} = \mathbf{r}_{ij}/r_{ij}$ with $r_{ij} = |\mathbf{r}_{ij}|$) experiences a force with the components of conservative interaction force F^C, dissipative force F^D, random force F^R, and bond force F^S, that is, $f_i = \sum_{j\neq i}(F_{ij}^C + F_{ij}^D + F_{ij}^R + F_{ij}^S)$ where the sum runs over all beads j. The conservative force is given by $F_{ij}^C = \alpha_{ij}\omega(r_{ij})\mathbf{e}_{ij}$, where α_{ij} is the maximum repulsion between beads i and j and has a linear relationship with Flory−Huggins χ parameter: $\chi_{ij} = (\alpha_{ij} - \alpha_{ii})/3.27$. A larger α corresponds to a stronger bead−bead repulsion, and α_{ii} is usually chosen to 25 for interactions between like species. For interactions between unlike beads, $\alpha_{AP} = \alpha_{BQ} = \alpha_{Ap} = \alpha_{Bq} = 15$, $\alpha_{AQ} = \alpha_{BP} = \alpha_{Aq} = \alpha_{Bp} = 40$, $\alpha_{PQ} = \alpha_{pq} = 30$, and $\alpha_{AB} = 80$, where the subscripts A, B are two fluid phases; P, Q are long chains tethered on one type of Janus particles; and p, q are short chains tethered on the other type of Janus particles. Clearly, the P and p chains have an affinity to the A domain while Q and q to the B domain. The repulsion between long and short tethers anchoring in the same phase domain, that is, α_{Pp} and α_{Qq} are chosen to 27. The weight function $\omega(r_{ij})$ is chosen as $\omega(r_{ij}) = 1 - r_{ij}/r_c$ for $r_{ij} < r_c$ and $\omega(r_{ij}) = 0$ for $r_{ij} \geq r_c$, where r_c is the truncate distance. The random force F_{ij}^R and the dissipative force F_{ij}^D are given by $F_{ij}^R = \sigma\omega(r_{ij})\xi_{ij}\Delta t^{-1/2}\mathbf{e}_{ij}$ and $F_{ij}^R = -1/2\sigma^2\omega(r_{ij})(\mathbf{v}_{ij}\cdot\mathbf{e}_{ij})\mathbf{e}_{ij}$, where $\mathbf{v}_{ij} = \mathbf{v}_i - \mathbf{v}_j$ and $\mathbf{v}_i$ denotes the velocity of bead i. ξ_{ij} is a random number which has zero mean and unit variance. The noise amplitude, σ, is fixed at $\sigma = 3$ in the present simulations. The bonds between the beads are represented by a harmonic spring potential $E_{bond} = K_{bond}((r - b)/r_c)^2$, where $K_{bond} = 64$ and $b = 0.5r_c$ are the bond constant and the equilibrium bond length, respectively.[32] The side lengths of the simulation box in x, y, and z directions are $40r_c$, $40r_c$, and $20r_c$ respectively, and with periodic boundary condition in all directions, which is large enough to avoid the finite size effect. The equilibrium structure is determined for several independent runs and after very long equilibration times with the traditional DPD algorithm.[31] Specially, mechanical pressure is exerted to the system by changing the lateral dimensions of our simulation box and simultaneously modifying the height of the box to keep the volume of the system constant,[36] that is, $(x, y, z) \rightarrow (\delta x, \delta y, z/\delta^2)$, as indicated by the arrows in Figure 1b.

dx.doi.org/10.1021/nl5029396 | Nano Lett. 2014, 14, 6910−6916

■ ASSOCIATED CONTENT

Supporting Information

Additional simulation results and videos. This material is available free of charge via the Internet at http://pubs.acs.org.

■ AUTHOR INFORMATION

Corresponding Author

*E-mail: ltyan@mail.tsinghua.edu.cn.

Author Contributions

†Z.L. and R. G. contributed equally.

Notes

The authors declare no competing financial interest.

■ ACKNOWLEDGMENTS

The authors thank Bojun Dong and Jian Mao for helpful discussions. This work is supported by the National Natural Science Foundation of China under Grants 21422403, 21174080, and 51273105.

■ REFERENCES

(1) Balazs, A. C.; Emrick, T.; Russell, T. P. *Science* **2006**, *314*, 1107−1110.
(2) Kotov, N. A.; Weiss, P. S. *ACS Nano* **2014**, *8*, 3101−3103 and references therein..
(3) Gupta, S.; Zhang, Q. L.; Emrick, T.; Balazs, A. C.; Russell, T. P. *Nat. Mater.* **2006**, *5*, 229−233.
(4) Mackay, M. E.; Tuteja, A.; Duxbury, P. M.; Hawker, C. J.; Horn, B. V.; Guanz, Z.; Chen, G.; Krishnan, R. S. *Science* **2006**, *311*, 1740−1743.
(5) Yan, L. T.; Xie, X. M. *Prog. Polym. Sci.* **2013**, *38*, 369−406.
(6) Curk, T.; Martinez-Veracoechea, F. J.; Frenkel, D.; Dobnikar, J. *Nano Lett.* **2014**, *14*, 2617−2622.
(7) Szleifer, I. *Biophys. J.* **1997**, *72*, 595−612.
(8) Rubinstein, B.; Coluzza, I.; Miller, M. *Phys. Rev. Lett.* **2012**, *108*, 208104.
(9) Davis, M. E.; Chen, Z. G.; Shin, D. M. *Nat. Rev.* **2008**, *7*, 771−782.
(10) Stuart, M. A. C.; Huck, W. T. S.; Genzer, J.; Müller, M.; Ober, C.; Stamm, M.; Sukhorukov, G. B.; Szleifer, I.; Tsukruk, V. V.; Urban, M.; Winnik, F.; Zauscher, S.; Luzinov, I.; Minko, S. *Nat. Mater.* **2010**, *9*, 101−113.
(11) Yoon, B.; Luedtke, W. D.; Barnett, R. N.; Gao, J.; Desireddy, A.; Conn, B. E.; Bigioni, T.; Landman, U. *Nat. Mater.* **2014**, *13*, 807−811.
(12) Böker, A.; He, J.; Emrick, T.; Russell, T. P. *Soft Matter* **2007**, *3*, 1231−1248.
(13) Chan, H.; Král, P. *Nanoscale* **2011**, *3*, 1881−1886.
(14) Hamer, M. J.; Iyer, B. V. S.; Yashin, V. V.; Balazs, A. C. *Nano Lett.* **2014**, *14*, 4745−4750.
(15) Bar-Segev, M.; Haick, H. *ACS Nano* **2013**, *7*, 8366−8378.
(16) Tokarev, I.; Minko, S. *Soft Matter* **2012**, *8*, 5980−5987.
(17) Yang, Y.; Ouyang, J.; Ma, L. P.; Tseng, R. J. H.; Chu, C. W. *Adv. Funct. Mater.* **2006**, *16*, 1001−1014.
(18) Li, G.; Zhu, R.; Yang, Y. *Nat. Photonics* **2012**, *6*, 153−161.
(19) Stamm, M.; Sommer, J. U. *Nat. Mater.* **2007**, *6*, 260−261.
(20) Cao, X. Z.; Merlitz, H.; Wu, C. X.; Sommer, J. U. *ACS Nano* **2013**, *7*, 9920−9926.
(21) Choueiri, R. M.; Klinkova, A.; Therien-Aubin, H.; Rubinstein, M.; Kumacheva, E. *J. Am. Chem. Soc.* **2013**, *135*, 10262−10265.
(22) Gupta, S.; Zhang, Q.; Emrick, T.; Russell, T. P. *Nano Lett.* **2006**, *6*, 2066−2069.
(23) Aldaye, F. A.; Palmer, A. L.; Sleiman, H. F. *Science* **2008**, *321*, 1795−1799.
(24) Shenhar, R.; Norsten, T. B.; Rotello, V. M. *Adv. Mater.* **2005**, *17*, 657−669.
(25) Chiu, J. J.; Kim, B. J.; Kramer, E. J.; Pine, D. J. *J. Am. Chem. Soc.* **2005**, *127*, 5036−5037.
(26) Kim, J. U.; Matsen, M. W. *Phys. Rev. Lett.* **2009**, *102*, 078303.
(27) Balazs, A. C. *Nat. Mater.* **2007**, *6*, 94−95.
(28) Zhang, D.; Carignano, M. A.; Sleifer, I. *Phys. Rev. Lett.* **2006**, *96*, 028701.
(29) Singh, C.; Ghorai, P. K.; Horsch, M. A.; Jackson, A. M.; Larson, R. G.; Stellacci, F.; Glotzer, S. C. *Phys. Rev. Lett.* **2007**, *99*, 226106.
(30) Sheiko, S. S.; Zhou, J.; Arnold, J.; Neugebauer, D.; Matyjaszewski, K.; Tsitsilianis, C.; Tsukruk, V.; Carrillo, J. M. Y.; Dobrynin, A. V.; Rubinstein, M. *Nat. Mater.* **2013**, *12*, 735−740.
(31) Groot, R. D.; Warren, P. B. *J. Chem. Phys.* **1997**, *107*, 4423−4435.
(32) Yan, L. T.; Popp, N.; Ghosh, S. K.; Böker, A. *ACS Nano* **2010**, *4*, 913−920.
(33) Kim, B. J.; Bang, J.; Hawker, C. J.; Chiu, J. J.; Pine, D. J.; Jang, S. G.; Yang, S. M.; Kramer, E. J. *Langmiur* **2007**, *23*, 12693−12703.
(34) Martin, T. B.; Dodd, P. M.; Jayaraman, A. *Phys. Rev. Lett.* **2013**, *110*, 018301.
(35) Kumar, S. K.; Jounault, N.; Benicewicz, B.; Neely, T. *Macromolecules* **2013**, *46*, 3199−3214.
(36) Groot, R. D.; Rabone, K. L. *Biophys. J.* **2001**, *81*, 725−736.
(37) Delaunay, B. N. *Izv. Akad. Nauk SSSR, Otd. Mat. Estestv. Nauk* **1934**, *7*, 793−800.
(38) Kusumaatmaja, H.; Wales, D. J. *Phys. Rev. Lett.* **2013**, *110*, 165502.
(39) Fejer, S. N.; Chakrabarti, D.; Kusumaatmaja, H.; Wales, D. J. *Nanoscale* **2014**, *6*, 9448−9456.
(40) Wang, B.; Bae, S. C.; Granick, S. *Nat. Mater.* **2012**, *11*, 481−485.
(41) Meyer, H.; Semenov, A. N. *Phys. Rev. Lett.* **2012**, *109*, 248304.
(42) Kim, J.; Kim, C.; Sung, B. J. *Phys. Rev. Lett.* **2013**, *110*, 047801.
(43) Binks, B. P.; Fletcher, P. D. I. *Langmuir* **2001**, *17*, 4708−4710.
(44) Kaganer, V. M.; Möhwald, H.; Dutta, P. *Rev. Mod. Phys.* **1999**, *71*, 779−819.
(45) Rubinstein, M.; Colby, R. H. *Polymer Physics*; Oxford University Press: Oxford, 2003.
(46) Flory, P. J. *Principles of Polymer Chemistry*; Cornell University Press: New York, 1953.
(47) Verma, A.; Uzun, O.; Hu, Y.; Hu, Y.; Han, H. S.; Watson, N.; Chen, S.; Irvine, D. J.; Stellacci, F. *Nat. Mater.* **2008**, *7*, 588−595.
(48) Arai, N.; Yasuoka, K.; Koishi, T.; Ebisuzaki, T.; Zeng, X. *J. Am. Chem. Soc.* **2013**, *135*, 8616−8624.